Original Article

The application value of ultra-short echo time MRI in the quantification of liver iron overload in a rat model

Qiaoling Wu[1], Xiuwei Fu[2], Zhizheng Zhuo[3], Mingfeng Zhao[4], Hongyan Ni[5]

[1]Tianjin University of Traditional Chinese Medicine, Tianjin 300192, China; [2]Department of Radiology, First Central Clinical College, Tianjin Medical University, Tianjin 300192, China; [3]Philips Healthcare, Beijing 100600, China; [4]Department of Hematology, [5]Department of Radiology, Tianjin First Central Hospital, Tianjin 300192, China

Correspondence to: Hongyan Ni, PhD. Department of Radiology, Tianjin First Central Hospital, Tianjin 300192, China. Email: nihyan@sina.com.

Background: The quantitative evaluation of liver iron concentration (LIC) is important in guiding the treatment of blood transfusion-dependent patients. Conventionally, LIC is assessed through R2*or R2 values using magnetic resonance imaging (MRI). However, most of the studies using MRI to determine iron overload were restricted by the minimum echo time, so that severe iron overload could hardly be quantified. In our study, we demonstrate a new approach to overcome the limitation of the shortest echo time using ultra-short echo time (UTE) MRI to quantify liver iron overload of varying degrees in a rat model.

Methods: Sixty female Sprague-Dawley rats were included and randomly assigned into 10 equal groups. Group 1 was not injected with iron dextran. Groups 2 to 10 were intraperitoneally injected with iron dextran at a dose of 15 mg/kg every 3 days. On every 6th day, one group was randomly selected from groups 2 to 10 for MRI scanning and liver iron concentration (LIC) detection. For groups 1 to 10, images were acquired by UTE sequence using a 3.0T MR scanner, and the T2* value and R2* value were obtained (R2* =1/T2*). In addition, LIC was measured using an atomic absorption photometer. The correlation analysis between R2* value and LIC was performed and the regression equation of R2* and LIC was established and its reliability verified.

Results: For groups 1 to 10, R2* values and LIC ranged from 60.16±4.76 to 1,306.90±42.26 Hz and from 0.84±0.11 to 5.89±2.64 mg/g dry, respectively. The R2* value was linearly correlated to the LIC ($r=0.897$, $P<0.001$), and the linear regression equation was LIC = 0.005 × R2* + 1.783. The validation analysis results showed that the intragroup correlation coefficient (ICC) between the predicted and measured LIC was 89.5%.

Conclusions: The UTE sequence could be used for quantification of varying degrees of hepatic iron overload in the rat model, and the LIC could be predicted by using the R2* value on an MR 3.0T scanner.

Keywords: Magnetic resonance imaging (MRI); ultra-short echo time; rat liver; iron overload

Submitted Aug 22, 2018. Accepted for publication Oct 23, 2018.
doi: 10.21037/qims.2018.10.11
View this article at: http://dx.doi.org/10.21037/qims.2018.10.11

Introduction

Hematologic diseases are common clinically, including myelodysplastic syndrome (MDS), severe β thalassemia, myelofibrosis (MF), and aplastic anemia (AA), and usually require long-term and repeated blood transfusions for treatment. However, this treatment strategy might lead to an excessive supply of iron, resulting in varying degrees of iron overload in different organs, especially in the liver (1,2). The liver is the most important organ for iron storage and metabolism of ferritin and hemosiderin. However, severe iron overload could cause liver fibrosis, cirrhosis, and even cancer (3); therefore, accurate measurement of hepatic iron is particularly important for monitoring the degree of iron

overload in the liver during the treatment of hematologic diseases.

Liver biopsy is the gold standard for the clinical detection of hepatic iron load. However, since the method is invasive, random, and poorly repeatable, it is not accepted by all patients. The concentration of serum ferritin (SF) is often used to indirectly reflect the degree of iron overload (4). However, previous studies (5,6) suggested that SF was likely to be affected by infection, malignant tumor, and inflammatory factors; thus, it might not be significantly associated with the level of hepatic iron. Although a superconducting quantum interference device (SQUID) was used for accurate quantitative measurement of hepatic iron (7), the very small number of devices in the world (only four) has restricted its application. For clinical imaging techniques, computed tomography (CT) could be used for the semi-quantitative detection of hepatic iron (8), but its clinical application is also limited due to high radiation and low repeatability.

In recent years, the use of MRI in quantitative measurement of liver iron has been widely recognized, and previous studies also confirmed the feasibility of T2 and T2* mapping in liver iron quantification (9,10). However, for patients with severe liver iron overload, the accurate T2* value might not be obtained due to the restriction of echo time (TE). Therefore, previous studies (11) failed to make a precise evaluation of severe iron overload, and the use of MRI in quantitative determination of liver iron content was also limited. In recent years, a new technique, the ultra-short echo time (UTE) sequence, which is primarily used for quantitative detection of the joint, skeletal muscle, and the lung (12-15), has been developed. However, some other studies also suggested that this sequence could be applied to the patients with hepatic iron overload, especially in severe iron deposits (16). To obtain a large number of biopsy and pathological results to verify the efficacy of this method for clinical application, we used rats to simulate iron deposition in the human body. To date, no animal experiments have been performed to compare R2* and the actual liver iron content by using the UTE sequence under 3.0 T MR.

In this study, we applied the UTE sequence on 3.0 T MR to scan rat models with different levels of hepatic iron deposition. The concentration of hepatic iron was also measured by atomic absorption photometer (17). Our study aimed to explore the application value of UTE sequence in quantitative determination of hepatic iron overload with different levels, and to provide reference for clinical use of UTE sequence in liver iron quantification.

Methods

Animal models of iron overload

Experiments were conducted on 8- to 10-week-old bacterial-pathogen-free female Sprague-Dawley rats. The rats were housed in a pathogen-free environment monitored by a sentinel animal. Rats had free access to water and standard rodent diet. The rats (n=60, 190–210 g) were randomly assigned into ten groups (n=6 per group) after 1 week of adaptive feeding. Group 1 was the non-iron injection group, and the others were iron-injection groups. In groups 2 to 10, the rats were intraperitoneally injected with iron dextran at a dose of 15 mg/kg every 3 days, and each rat was weighed and observed for its general condition (fur and feeding) before injection. On every 6th day, one group was randomly selected and given common feeding to allow sufficient iron deposition. Then, the rats were anesthetized and MRI scanning with the UTE sequence was performed. After MRI scanning, rats underwent dissection to remove the liver tissue for iron determination; then, the rats were euthanized. The animal facilities and handling conformed to the National Institutes of Health Guide for the Care and Use of Laboratory Animals. The investigation was approved by the Institutional Animal Care and Use Committee at the Tianjin First Central Hospital.

MRI acquisition and post-processing

All studies were performed on a Philips Ingenia 3.0T MRI system with a dStream 4-channel rat coil. CO_2 was used to anesthetize the animals. The rat liver was fixed in the center of the animal coil with a bandage to reduce respiratory motion artifacts, and rats remained free to breathe during the scanning.

UTE imaging was performed using a three-dimensional (3D) gradient echo sequence with radial acquisition. The parameters of the UTE protocol were as follows: the first echo time (TE1) =0.56 ms, echo spacing =3.0 ms, repetition time (TR) =22 ms, flip angle =15°, field of view (FOV) =60 mm × 60 mm, pixel size =0.4 mm × 0.4 mm, slice thickness =1.5 mm, no slice gap, and slice number =20.

The T2* map was calculated by a home-developed Matlab code after the image registration for different echoes. Two radiologists measured the T2* value of different regions of interest (ROIs) using the MRIcron software, and the difference between the measured results should be within 5%. To avoid inhomogeneous iron deposition, we selected the level of the largest hepatic area

and avoided large vessels and bile ducts. Five circular ROIs with the same diameter (1 cm) were drawn, and the average R2* [R2*(HZ) =1,000/T2* (ms)] value was obtained for further statistical analysis.

Determination of liver iron content using atomic absorption spectroscopy

Sample processing

After the rats were euthanized, their livers were sampled. We removed the large vessels and bile ducts, washing them with ultrapure water for several times, weighing, and drying in a 60 ℃ oven for 72 hours until constant weight.

Then, the tissue was ground into powder, and 0.1 g of the powder was weighed by an analytical balance, placed in a beaker. Five mL of mixed acid (nitric acid:perchloric acid =4:1) was added, and the beaker was placed still overnight. Afterward, the mixture was water-bath heated until clear.

Standard solution

Standard stock solution (25 mg/L) was prepared using the standard iron solution (1 mg/mL), and the stock solution was further diluted into standard work solutions, with iron concentrations of 0.5, 2, 4, 8, 12, and 20 mg/L, respectively [y=38.78× (–1.69), correlation coefficient r=0.99237; the standard curve had good linearity]. Ultrapure water was used for the dilution of all solutions.

Working conditions of the atomic absorption photometer

Hepatic iron determination was performed using the flame method (17), and parameters for the atomic absorption photometer are as follows: the element is Fe; negative pressure is 463.5 V. We used a lamp current of 4 mA, a working wave length of 248.33 nm, a band width of 0.2 nm, a gas flow of 2,300 ($mL \cdot min^{-1}$), a height of 8 mm, an integration time of 1 s, and a filter coefficient of 0.6. The calculation mode was continuous. The flame method was performed to determine iron content in the digested rat liver.

Statistical analysis

Statistical analysis was performed using the SPSS 17.0 software. Measurement data are presented as mean ± standard deviation (SD). All data were tested by a one-sample Kolmogorov-Smirnov test for normal distribution. For data that did not fit the normal distribution, correlation analysis of the R2* value and LIC were performed using the Spearman method. From each group, 5 of the 6 rats were randomly selected (50 rats total) to calculate the regression equation between the R2* value and LIC, and the remaining rats in each group (10 rats total) were used for validation. The R2* values of the validation were fitted into the regression equation to calculate the predicted value of LIC (LIC_p), and intragroup reliability analysis was performed to compare the LIC_p with the tested value of LIC (LIC_t), thus verifying the conformity between the value predicted by the equation and the value obtained from the test. Statistical significance was defined at $P \leq 0.05$.

Results

General condition

Fur color: with prolonged time of administration, rats in groups 1 to 10 all had coarse and thin, lackluster fur. Their claws, ears, and tails turned red gradually.

Bodyweight: with prolonged time of administration and increased amount of iron deposition, rats showed a decrease in diet, with no increase or decrease in body weight.

Activity: with prolonged time of administration and increased amount of iron deposition, rats had reduced activity, and they were sluggish and slow to react.

MRIs

Along with the increase of administration time, rats in groups 1 to 10 all showed a decreased trend in MRI signal intensity. *Figure 1* shows the MR-UTE images of varying degrees of iron overload in four groups of rats (group 1: not injected with the iron dextran; group 4: injected with iron dextran for 24 d, mild iron overload; group 7: injected with iron dextran for 42 d, moderate iron overload; group 10: injected with iron dextran for 60 d, severe iron overload). As the results show, the MRI signals of the liver decreased gradually (*Figure 1*).

The R2 value and LIC for model rats*

After image processing, the T2* value was obtained, and the R2* value was calculated by the formula R2* =1/T2*. For

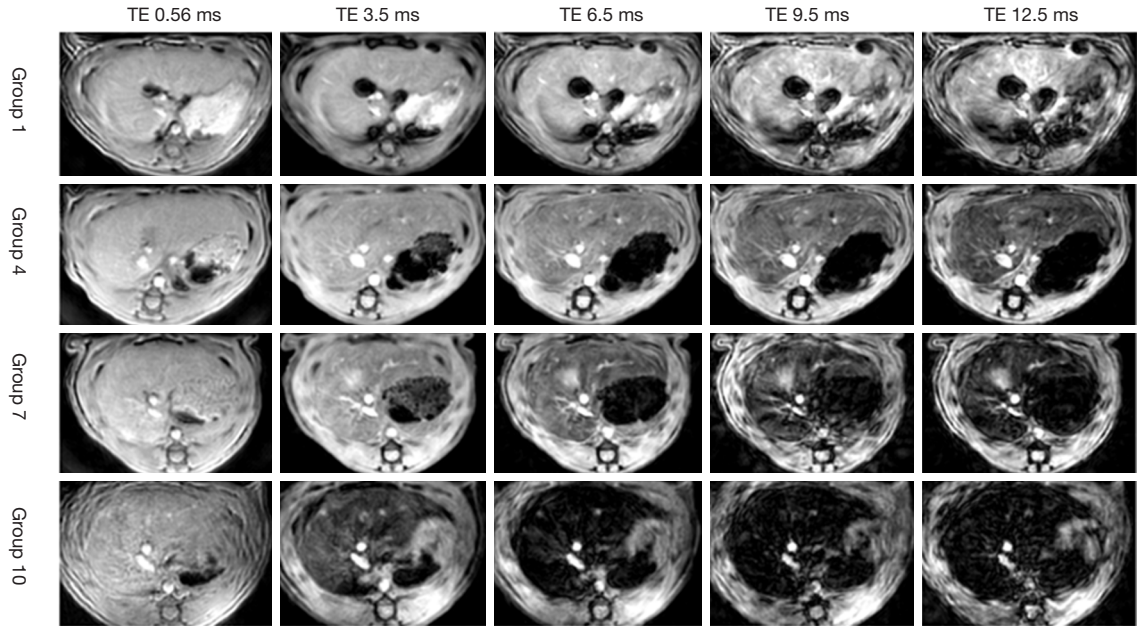

Figure 1 MR-UTE images with different echo times (0.56–12.5 ms) of the rats with varying degrees of liver iron overload. With the iron deposition degree increasing, the liver MRI signals decreased gradually. Group 1: without injection of the iron dextran; group 4: injected with iron dextran for 24 d, mild iron overload; group 7: injected with iron dextran for 42 d, moderate iron overload; group 10: injected with iron dextran for 60 d, severe iron overload.

Table 1 The calculation of R2* value and LIC in rat liver

Groups	R2* value (Hz)	LIC (mg/g dry)
1	60.16±4.76	0.84±0.11
2	108.96±8.35	2.16±0.18
3	125.11±28.9	2.14±0.59
4	161.19±25.8	2.36±0.41
5	152.12±31.4	2.58±0.64
6	218.80±12.30	3.30±0.11
7	331.80±66.70	4.05±0.74
8	413.62±96.50	4.01±0.33
9	530.00±180.30	4.83±0.18
10	1,306.90±42.26	5.89±2.64

LIC, liver iron concentration.

all groups, the R2* value was within the following range: 60.16±4.76 to 1,306.90±42.26 Hz (*Table 1*).

The LIC was determined using the atomic absorption photometer, and the LIC of rats in groups 1 to 10 ranged within 0.84±0.11 to 5.89±2.64 mg/g dry (*Table 1*).

Correlation analysis between the R2 value and LIC*

Correlation analysis between the R2* value and LIC was performed for all rats. The analysis obtained a correlation coefficient of r=0.897, and a P<0.001, which indicated that LIC was highly correlated with the R2* value. *Figure 2* shows the scatter plot of the R2* value and LIC for all rats.

Logistic regression and validation

Five rats were randomly selected from each group, so that a total of 50 rats were assigned into the experimental group, and logistic regression analysis was performed to obtain the regression equation between the R2* value and the LIC. With a slope of 0.005 and an intercept of 1.783, the regression equation of R2* and LIC was calculated as:

$$LIC = 0.005 \times R2^* + 1.783 \quad [1]$$

The remaining rats in each group (10 total) were assigned into the validation group, and their R2* values were fitted into Eq. [1] to obtain the LIC_p. The LIC_p was further

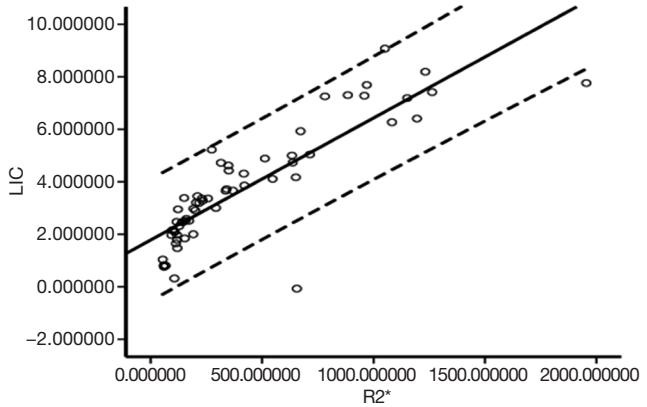

Figure 2 The scatter plot of R2* value and LIC for all rats. The solid line represents the fitting straight line, and the dotted line represents the 95% confidence interval. The result suggested significant positive correlation. LIC, liver iron concentration.

compared with the LIC_t to verify the intragroup reliability of the formula, and the intragroup correlation coefficient (ICC) was 89.5%, which indicated high consistency.

Discussion

In our study, we established a rat liver iron overload model to explore the value of MR-UTE sequence in the quantitative detection of iron deposition of different degrees in the liver of rats. The results showed that the MR-UTE sequence has advantages in quantifying severe liver iron overload. The R2* value is highly positively correlated with LIC. The regression equation was obtained by linear regression analysis between R2* and LIC. The LIC could be predicted using the R2* value. In this experiment, we verify the application value of MR-UTE sequence in the quantitative detection of liver iron overload, and partially solve the problem that liver severe iron overload cannot be accurately quantified.

The use of MR-UTE sequence in liver iron overload has provided a new insight for quantitative determination of severe iron overload. Previously, the UTE sequence was mainly used for the examination of musculoskeletal joints or lungs (12-15), and its application in the liver was less common. In recent years, studies using MRI to determine iron overload were all restricted by the minimum TE time, so that severe iron overload could hardly be quantified. For example, Paisant (11) performed the signal intensity ratio (SIR) method to measure liver iron overload on 3.0T MR, and the minimum TE was 1.15 ms. Sharma (18,19) used Quantitative Susceptibility Mapping (QSM) to quantify liver iron overload, and the minimum TE was 1.2 ms. Both Jackson (20) and Carpenter (21) mentioned that the quantification of myocardial iron overload was restricted by the minimum echo time. Therefore, Hong (22) and Wang *et al.* (23) constructed a nanoparticle model with different amounts of iron oxide and verified the feasibility of UTE sequence in determining the iron content under 3.0T field strength, which did not mimic human physiological metabolism. Krafft *et al.* (24) evaluated the liver iron quantification with UTE sequence on 1.5T MR and found that the hepatic iron concentration could be quantified, but the relaxation time obtained by 1.5T MR is not suitable for 3.0T MR. In this study, rat models with different levels of hepatic iron deposition were scanned with UTE sequence on a 3.0 MR. On the premise of guaranteeing image quality, the application of MR-UTE sequence shortened the first TE to 0.56 ms, which facilitated the analysis of severe iron overload in the liver of Sprague-Dawley rats and achieved quantified determination of iron overload from mild to severe.

This study applied the MR-UTE sequence to quantify mild, moderate, and severe iron overload in the liver of rats, and found that the R2* value was highly correlated to the value of LIC measured by the atomic absorption photometer. Peng (25) built a rabbit iron overload model and verified the correlation of liver iron overload with the T2* value measured by MR gradient echo sequence. Yet, due to the restriction of minimum TE, the study only analyzed the situation of mild and moderate iron deposition. Some *in vivo* studies (26-28) found that the R2* was significantly correlated with the LIC for mild and moderate hepatic iron overload. Krafft (24) and Hong (22) verified the significant correlation between the R2* value measured by MR-UTE and the actual level of iron deposition in mild, moderate, and severe iron overload, with a correlation coefficient r=0.9537. In this study, due to the influence of metabolic and individual differences, the R2* value acquired by the UTE sequence was correlated to the LIC with a r=0.897, which indicated that the R2* value obtained from MR-UTE scanning was highly correlated to LIC, and that the use of UTE in quantifying liver iron overload is feasible and is of advantage when it comes to the quantification of severe iron overload.

This study also established a regression equation between the R2* value and the LIC, and verified its reliability by fitting data of the validation group into the equation. Therefore, R2* obtained from 3.0T MR can be converted

to LIC, and made it possible to use the R2* value to predict the concentration of hepatic iron. Paisant (11) established a regression equation of LIC = (0.0254× R2*) +0.202 when studying hepatic iron overload in patients with thalassemia. In our study, a regression equation of LIC = 0.005× R2* +1.783 was obtained by adopting the iron overload model of rats, which eliminated the interference of basic diseases, such as liver fibrosis, and broke through the limitation of the shortest echo time. The slope of our regression equation is different from the result of Paisant (11), which may be caused by field strength (3.0T is different from 1.5T), scanning sequence parameters, and the physiological differences between a rat model and human liver cases. Moreover, a validation experiment was performed to verify the reliability of the regression equation, and the result suggested that the R2* value obtained from 3.0T MR could be used as a reliable factor to predict the concentration of hepatic iron.

The Sprague-Dawley rats were selected as the modeling subjects in this study because they could better simulate iron deposition in the human body and, presently, they are widely used as experimental animals in clinical studies. Wood *et al.* (29) constructed a gerbil model when studying myocardial iron overload, and they also used iron dextran as we did in this study. However, Sprague-Dawley rats were used in our study, because they are larger than gerbils, providing a better image signal-to-noise ratio to ensure the accuracy of the R2* measurement. Our study emphasized the dynamic progression of hepatic iron overload from mild to severe. Rats in groups 1 to 10 had a LIC ranging from 0.84±0.11 to 5.89±2.64 mg/g dry, and a R2* value from 60.16±4.76 to 1,306.9±42.26 Hz, which indicated that the model successfully simulated the process of iron overload from mild to severe. Further, MR scanning and liver sampling were performed on the same day, which aimed to guarantee the consistency of experiments and avoid the influence of other factors such as different metabolism in different time.

Actually, iron overload does cause changes in both T1 and T2* values. However, we only focus on the variation of T2* values with different LIC, and do not pay attention to T1 in our study, because iron mainly affects the change of T2* value; T2* value quantitative iron overload is more sensitive than T1. Henninger *et al.* (30) found important additional information may be obtained by the combination of T1 and T2* mapping. They found that 53% of patients with hepatic iron deposition had reduced T1 relaxation time. But T2* relaxation was very accurate in diagnosing hepatic iron overload. Iron overload mainly affects the liver parenchyma, and the large blood vessels and bile ducts in the liver may affect the accuracy of the measurement. Therefore, we chose to place five small ROIs in different liver parenchyma, and take the average value as the T2* value of the whole liver; we then converted to the R2* value based on the relationship between T2* and R2*(R2* =1/T2*).

However, this study has some limitations. One study suggested that the presence of fat would affect accurate measurement of iron overload (31). Because the fatty layer of rat is relatively thin, the impact of fat on determination of iron overload may be tiny or negligible; thus, the fat signal was not suppressed in our study. In the following studies, we will do some UTE sequences with and without suppression in patients with iron overload to further explore the effect of fat on iron deposition. Second, to ensure the image quality and the accuracy of measurements, we set TE1 =0.56 ms; TE1 may be set shorter as the UTE sequence is further optimized and the MR system is further developed. Third, the regression equation cannot be directly applied to clinical practice, because the iron storage and the ultimate iron tolerance of rats are lower than in normal humans; thus, the R2* value of the liver obtained in this experiment is lower than that of patients with iron overload of the same degree. We will collect iron overload patients with liver biopsy gradually to explore the application value of UTE sequence in patients with liver iron overload, and fit the regression equation of LIC and R2* value in patients with liver iron overload to further expand its application in clinical detection.

In conclusion, this study confirmed the feasibility and value of the UTE sequence in determining hepatic overload by constructing the rat model of iron overload, and achieved the calculation of LIC using the R2* value in rat model. This provided experimental basis for the use of UTE in clinical detection of varying degrees of liver iron overload, and we believe the UTE sequence would have a broad application with the deepening of clinical studies.

Acknowledgements

Funding: This study has received funding by the Tianjin Health and Family Planning Commission (grant no. 15KG134, grant no. 16KG110), and Tianjin Natural Science Foundation (grant no. 17JCZDJC35800).

Footnote

Conflicts of Interest: The authors have no conflicts of interest

to declare.

Ethical Statement: The investigation was approved by the Institutional Animal Care and Use Committee at the Tianjin First Central Hospital.

References

1. Nam H, Wang CY, Zhang L, Zhang W, Hojyo S, Fukada T, Knutson MD. ZIP14 and DMT1 in the liver, pancreas, and heart are differentially regulated by iron deficiency and overload: implications for tissue iron uptake in iron-related disorders. Haematologica 2013;98:1049-57.
2. Porter JB, Garbowski M. The Pathophysiology of Transfusional Iron Overload. Hematol Oncol Clin North Am 2014;28:683-701.
3. Pietrangelo A. Metals, oxidative stress, and hepatic fibrogenesis. Semin Liver Dis 1996;16:13-30.
4. Majd Z, Haghpanah S, Ajami GH, Matin S, Namazi H, Bardestani M, Karimi M. Serum Ferritin Levels Correlation With Heart and Liver MRI and LIC in Patients With Transfusion-Dependent Thalassemia. Iran Red Crescent Med J 2015;17:e24959.
5. Cippà PE, Boucsein I, Adams H, Krayenbuehl PA. Estimating Iron Overload in Patients with Suspected Liver Disease and Elevated Serum Ferritin. Am J Med 2014;127:1011.e1-3.
6. Shamsian BS, Esfahani SA, Milani H, Akhlaghpoor S, Mojtahedzadeh S, Karimi A, Shamshiri AR, Alavi S, Safari A, Rezaei N, Arzanian MT. Magnetic resonance imaging in the evaluation of iron overload: a comparison of MRI, echocardiography and serum ferritin level in patients with beta-thalassemia major. Clin Imaging 2012;36:483-8.
7. Jacobi N, Herich L. Measurement of liver iron concentration by superconducting quantum interference device biomagnetic liver susceptometry validates serum ferritin as prognostic parameter for allogeneic stem cell transplantation. Eur J Haematol 2016;97:336-41.
8. Luo XF, Yang Y, Yan J, Xie XQ, Zhang H, Chai WM, Wang L, Schmidt B, Yan FH. Virtual iron concentration imaging based on dual-energy CT for noninvasive quantification and grading of liver iron content: An iron overload rabbit model study. Eur Radiol 2015;25:2657-64.
9. Sanches-Rocha L, Serpa B, Figueiredo E, Hamerschlak N, Baroni R. Comparison between multi-echo T2* with and without fat saturation pulse for quantification of liver iron overload. Magn Reson Imaging 2013;31:1704-8.
10. Wahidiyat PA, Liauw F, Sekarsari D, Putriasih SA, Berdoukas V, Pennell DJ. Evaluation of cardiac and hepatic iron overload in thalassemia major patients with T2* magnetic resonance imaging. Hematology 2017;22:501-7.
11. Paisant A, Boulic A, Bardou-Jacquet E, Bannier E, d'Assignies G, Laine F, Turlin B, Gandon Y. Assessment of liver iron overload by 3 T MRI. Abdom Radiol (NY) 2017;42:1713-20.
12. C A Araujo E, Azzabou N, Vignaud A, Guillot G, Carlier PG. Quantitative ultrashort TE imaging of the short-T2 components in skeletal muscle using an extended echo-subtraction method. Magn Reson Med 2017;78:997-1008.
13. Sheikh K, Guo F, Capaldi DP, Ouriadov A, Eddy RL, Svenningsen S, Parraga G, Canadian Respiratory Research N. Ultrashort echo time MRI biomarkers of asthma. J Magn Reson Imaging 2017;45:1204-15.
14. Ma LH, Meng QF, Cheng YM. Discussion on factors affecting the quality of images of T2 component of MR 3D UTE double echo pulse sequence. Chinese Journal of Radiology 2011;45:388-91.
15. Tibiletti M, Paul J, Bianchi A, Wundrak S, Rottbauer W, Stiller D, Rasche V. Multistage three-dimensional UTE lung imaging by image-based self-gating. Magn Reson Med 2016;75:1324-32.
16. Doyle EK, Toy K, Valdez B, Chia JM, Coates T, Wood JC. Ultra-short echo time images quantify high liver iron. Magn Reson Med 2018;79:1579-85.
17. Soltan ME, Rageh HM, Rageh NM, Ahmed ME. Experimental approaches and analytical technique for determining heavy metals in fallen dust at ferrosilicon production factory in Edfu, Aswan, Egypt. Journal of Zhejiang University Science B 2005;6:708-18.
18. Sharma SD, Fischer R, Schoennagel BP, Nielsen P, Kooijman H, Yamamura J, Adam G, Bannas P, Hernando D, Reeder SB. MRI-based quantitative susceptibility mapping (QSM) and R2* mapping of liver iron overload: Comparison with SQUID-based biomagnetic liver susceptometry. Magn Reson Med 2017;78:264-70.
19. Sharma SD, Hernando D, Horng DE, Reeder SB. Quantitative susceptibility mapping in the abdomen as an imaging biomarker of hepatic iron overload. Magn Reson Med 2015;74:673-83.
20. Jackson LH, Vlachodimitropoulou E, Shangaris P, Roberts TA, Ryan TM, Campbell-Washburn AE, David AL, Porter JB, Lythgoe MF, Stuckey DJ. Non-invasive MRI biomarkers for the early assessment of iron overload in a humanized mouse model of beta-thalassemia. Sci Rep 2017;7:43439.

21. Carpenter JP, He TG, Kirk P, Roughton M, Anderson LJ, de Noronha SV, Baksi AJ, Sheppard MN, Porter JB, Walker JM, Wood JC, Forni G, Catani G, Matta G, Fucharoen S, Fleming A, House M, Black G, Firmin DN, St Pierre TG, Pennell DJ. Calibration of myocardial T2 and T1 against iron concentration. J Cardiovasc Magn Reson 2014;16:62.
22. Hong W, He Q, Fan SJ, Carl M, Shao HD, Chen J, Chang EY, Du J. Imaging and quantification of iron-oxide nanoparticles (IONP) using MP-RAGE and UTE based sequences. Magn Reson Med 2017;78:226-32.
23. Wang L, Potter WM, Zhao Q. In vivo quantification of SPIO nanoparticles for cell labeling based on MR phase gradient images. Contrast Media Mol Imaging 2015;10:43-50.
24. Krafft AJ, Loeffler RB, Song RT, Tipirneni-Sajja A, McCarville MB, Robson MD, Hankins JS, Hillenbrand CM. Quantitative Ultrashort Echo Time Imaging for Assessment of Massive Iron Overload at 1.5 and 3 Tesla. Magn Reson Med 2017;78:1839-51.
25. Peng P, Huang ZK, Long LL, Zhao FY, Li CY, Li WM, He TG. Liver Iron Quantification by 3 Tesla MRI: Calibration on a Rabbit Model. J Magn Reson Imaging 2013;38:1585-90.
26. d'Assignies G, Paisant A, Bardou-Jacquet E, Boulic A, Bannier E, Laine F, Ropert M, Morcet J, Saint-Jalmes H, Gandon Y. Non-invasive measurement of liver iron concentration using 3-Tesla magnetic resonance imaging: validation against biopsy. Eur Radiol 2018;28:2022-30.
27. St Pierre TG, Clark PR, Chua-Anusorn W, Fleming AJ, Jeffrey GP, Olynyk JK, Pootrakul P, Robins E, Lindeman R. Noninvasive measurement and imaging of liver iron concentrations using proton magnetic resonance. Blood 2005;105:855-61.
28. Hankins JS, McCarville MB, Loeffler RB, Smeltzer MP, Onciu M, Hoffer FA, Li CS, Wang WC, Ware RE, Hillenbrand CM. R2* magnetic resonance imaging of the liver in patients with iron overload. Blood 2009;113:4853-5.
29. Wood JC, Otto-Duessel M, Aguilar M, Nick H, Nelson MD, Coates TD, Pollack H, Moats R. Cardiac iron determines cardiac T2*, T2, and T1 in the gerbil model of iron cardiomyopathy. Circulation 2005;112:535-43.
30. Henninger B, Kremser C, Rauch S, Eder R, Zoller H, Finkenstedt A, Michaely HJ, Schocke M. Evaluation of MR imaging with T1 and T2* mapping for the determination of hepatic iron overload. Eur Radiol 2012;22:2478-86.
31. Sharma P, Altbach M, Galons JP, Kalb B, Martin DR. Measurement of liver fat fraction and iron with MRI and MR spectroscopy techniques. Diagn Interv Radiol 2014;20:17-26.

Cite this article as: Wu Q, Fu X, Zhuo Z, Zhao M, Ni H. The application value of ultra-short echo time MRI in the quantification of liver iron overload in a rat model. Quant Imaging Med Surg 2019;9(2):180-187. doi: 10.21037/qims.2018.10.11

